Bioorganic & Medicinal Chemistry 20 (2012) 6048–6058

Contents lists available at SciVerse ScienceDirect

Bioorganic & Medicinal Chemistry

journal homepage: www.elsevier.com/locate/bmc

Design, modification and 3D QSAR studies of novel 2,3-dihydrobenzo[*b*][1,4]dioxin-containing 4,5-dihydro-1*H*-pyrazole derivatives as inhibitors of B-Raf kinase

Yu-Shun Yang [†], Qing-Shan Li [†], Shuai Sun, Yan-Bin Zhang, Xiao-Liang Wang, Fei Zhang, Jian-Feng Tang, Hai-Liang Zhu [*]

State Key Laboratory of Pharmaceutical Biotechnology, Nanjing University, Nanjing 210093, People's Republic of China

ARTICLE INFO

Article history:
Received 17 July 2012
Revised 20 August 2012
Accepted 21 August 2012
Available online 30 August 2012

Keywords:
Dioxin
Modification
Pyrazole
Antitumor activity
B-Raf

ABSTRACT

Two series of novel 2,3-dihydrobenzo[*b*][1,4]dioxin-containing 4,5-dihydro-1*H*-pyrazole derivatives **C1–C15** and **D1–D15** have been synthesized and evaluated for their B-Raf inhibitory and anti-proliferation activities. Compound **C14** ((3-(4-bromophenyl)-5-(2-fluorophenyl)-4,5-dihydro-1*H*-pyrazol-1-yl)(2,3-dihydrobenzo[*b*][1,4]dioxin-6-yl)methanone) showed the most potent biological activity against B-Raf^{V600E} (IC_{50} = 0.11 μM) and WM266.4 human melanoma cell line (GI_{50} = 0.58 μM), being comparable with the positive control Erlotinib and more potent than our previous best compound, while **D10** ((2,3-dihydrobenzo[*b*][1,4]dioxin-2-yl)(5-(3-fluorophenyl)-3-phenyl-4,5-dihydro-1*H*-pyrazol-1-yl)methanone) performed the best in the **D** series (IC_{50} = 1.70 μM; GI_{50} = 1.45 μM). The docking simulation was performed to analyze the probable binding models and poses and the QSAR model was built for reasonable design of B-Raf inhibitors in future. The introduction of 2,3-dihydrobenzo[*b*][1,4]dioxin structure reinforced the combination of our compounds and the receptor, resulting in progress of bioactivity.

1. Introduction

Being the second cause of mortality in the world, cancer is continuing to act as a major problem of health in both developing and developed countries.[1]Despite the progress in medicine, the commitment to the laborious task of discovering new anticancer agents remains critically important.

As part of the mitogen-activated protein kinase pathway (MAPK), Raf kinases exist in three isoforms, A-Raf, B-Raf and C-Raf (Raf-1), and have been indicated to be critical for mediating cell proliferation and survival.[2,3] While the Ras-Raf-MEK-ERK pathway has been implicated in up to 30% of human cancers, activating mutations in Raf have been observed in melanoma (50–70%), thyroid cancers (40–70%) and ovarian cancer (50–70%).[4–6] Thus, the serine/threonine kinase B-Raf, which is mutated in 7% of human cancers, has drawn much attention. The most frequent mutation in B-Raf, which is found in the activation segment of the B-Raf kinase domain, is the valine for glutamic acid substitution (V600E),[7,8] accounting for a 500-fold increase in the basal rate of MEK phosphorylation over wild-type B-Raf and making B-Raf an attractive target for therapeutic intervention.[9]

Potent and selective B-Raf inhibitors have been developed constantly. Several small molecules, such as sorafenib,[10] PLX4720,[11] AZ628[12] and SB-590885,[13] have entered clinical or preclinical trials. Among the inhibitors above, SB-590885 inhibits B-Raf kinase activity with a K_i value of 0.16 nmol/L, which is 100-fold more potent than sorafenib. SB-590885 is a novel triarylimidazole derivative and the origin of its selectivity for B-Raf is probably due to its interactions with several B-Raf amino acids and then the presence of the indane-oxime. The particular situation is the interactions between a phenylalanine residue (PHE583) in the COOH-terminal lobe and both imidazole and pyridine rings of SB-590885.[13]

With a wide range of pharmaceutical and agrochemical activities, 4,5-dihydropyrazoles act as a significant class of heterocyclic biological agents.[14–16] Despite their anticancer activity through other pathways, some dihydropyrazole derivatives are also considered to be potent and selective inhibitors of B-Raf^{V600E} with sound IC_{50} values and have been identified by high-throughput screening.[17]

In our previous research, a series of 4,5-dihydropyrazole derivatives containing niacinamide moiety were synthesized and a QSAR model was built to discuss the structure–activity

Abbreviations: B-Raf, V-Raf murine sarcoma viral oncogene homologue B1; B-Raf^{V600E}, V600E mutant B-Raf; B-Raf^{WT}, B-Raf wild-type; IC_{50}, half maximal inhibitory concentration; GI_{50}, the concentration that causes 50% growth inhibition; QSAR, quantitative structure–activity relationship.

* Corresponding author. Tel./fax: +86 25 8359 2672.
E-mail address: zhuhl@nju.edu.cn (H.-L. Zhu).

† These authors contributed equally to the work.

0968-0896/$ - see front matter © 2012 Elsevier Ltd. All rights reserved.
http://dx.doi.org/10.1016/j.bmc.2012.08.043

relationship.[18] As shown in the result of 3D-QSAR in Figure 1, an increasing activity might be obtained by replacing the niacinamide moiety with a slightly larger template which can cause a lower electron density. Thus, we brought in the appropriate template of 1,4-benzodioxan, which is found in a variety of anticancer drugs with excellent bioavailability and low cytotoxicity.[19–22] Fulfilling the requirement of previous study, the modification in this paper also creates new possibility to reinforce the combination between our compounds and the receptor for the addition of nucleophilic structure can contribute to the formation of hydrogen bonds. According to the studies above, two novel series of 2,3-dihydrobenzo[*b*][1,4]dioxin-containing 4,5-dihydro-1*H*-pyrazole derivatives were designed as potential B-Raf^{V600E} inhibitors and predicted to have a positive progress with a sound cancer therapeutic benefit. Moreover, we conducted the comparison and discussion of not only the electronic situation but also the position of substitutes, which was complementary work of the previous research.

2. Results and discussion

2.1. Chemistry

Thirty 2,3-dihydrobenzo[*b*][1,4]dioxin-containing 4,5-dihydro-1*H*-pyrazole derivatives were synthesized to be screened for the antitumor activity. All of them were synthesized for the first time. The synthesis of compounds **C1–C15; D1–D15** followed the general pathway outlined in Scheme 1. They were both prepared in two methods. One method consists of three steps while the second consists of four. As for method I, firstly, different substituted acetophenone on treatment with substituted benzaldehyde in presence of 40% NaOH yielded different analogues of chalcones (**A**). Secondly, the cyclization of the obtained shiny powder by subjoining hydrazine hydrate led to 3,5-diaryl-4,5-dihydro-1*H*-pyrazole (intermediates **Ba**). Then, in the presence of EDCI and HOBt, the corresponding target compounds **C1–C15** (2,3-dihydrobenzo[*b*][1,4]dioxin-6-yl)(3,5-diaryl-4,5-dihydro-1*H*-pyrazol-1-yl) methanone and **D1–D15** (2,3-dihydrobenzo[*b*][1,4]dioxin-2-yl) (3,5-diaryl-4,5-dihydro-1*H*-pyrazol-1-yl)methanone were produced after being treated with 2,3-dihydrobenzo[*b*][1,4]dioxin-6-carboxylic acid and 2,3-dihydrobenzo[*b*][1,4]dioxin-2-carboxylic acid, respectively. As for method II, the first step was exactly the same as that of method I. While the second stage was the esterification of 2,3-dihydrobenzo[*b*][1,4]dioxin-6-carboxylic acid or 2,3-dihydrobenzo[*b*][1,4]dioxin-2-carboxylic acid with ethanol and 98% sulfuric acid. The third step was the hydrazinolysis to obtain corresponding hydrazide derivatives (**Bb**). Finally the target compounds **C1–C15** and **D1–D15** were produced after a cyclization of chalcones and corresponding hydrazide derivatives. The refined compounds were finally obtained by subsequent purification with recrystallisation. All of the synthetic compounds gave satisfactory analytical and spectroscopic data, which were full accordance with their depicted structures.

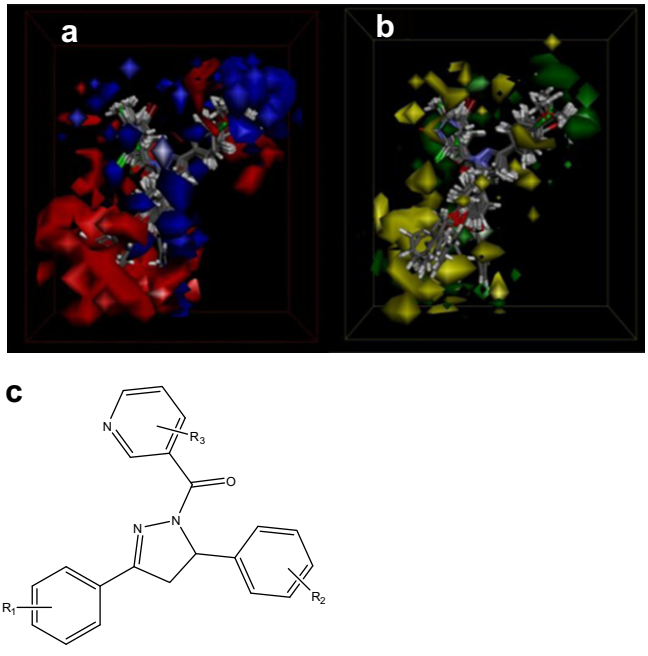

Figure 1. 3D-QSAR of 4,5-dihydropyrazole derivatives containing niacinamide moiety. (a) Red contours mean high electron density is expected to increase activity while blue contours mean low electron density is better. (b) Green areas mean steric bulk is better while yellow areas mean small groups are helpful. (c) The chemical structures of 4,5-dihydropyrazole derivatives containing niacinamide moiety.

2.2. Bioassay

All the synthesized compounds **C1–C15**, **D1–D15** were evaluated for their B-Raf^{V600E} inhibitory activities. The results were expressed as concentrations of IC_{50} (the half maximal inhibitory concentration of B-Raf^{V600E} mediated MEK phosphorylation) and GI_{50} (the half maximal inhibitory concentration of WM266.4 human melanoma cell line growth) and presented in Table 1. Meanwhile, we took compound **C0**, which has shown the best B-raf^{V600E} inhibitory activity in the previous research,[18] as another comparison to evaluate our modification. The results revealed that most of the synthetic compounds exhibited significant B-raf^{V600E} inhibitory activities and the structurally modification brought a relatively distinct progress.

The same as the previous study,[18] the activity data suggested that GI_{50} values of these compounds shared a similar tendency with their relevant IC_{50} values, which convinced the former inference that the anti-proliferative effect was produced by inhibitory action against B-Raf.

Out of the thirty 2,3-dihydrobenzo[*b*][1,4]dioxin-containing 4,5-dihydro-1*H*-pyrazole derivatives, compounds **C14** displayed the most potent activity with corresponding IC_{50} value of 0.11 μM and GI_{50} value of 0.58 μM, being comparable with the positive control Erlotinib (IC_{50} = 0.06 μM and GI_{50} = 8.12 μM) and obviously more potent than our previous best compound **C0** (IC_{50} = 0.20 μM and GI_{50} = 0.80 μM). Meanwhile, compound **D10** displayed most potent activity in the **D** series, with relevant IC_{50} value of 1.70 μM and GI_{50} value of 1.45 μM, which was also comparable with Erlotinib although not so good as **C14**. This fact indicated that the introduction of 2,3-dihydrobenzo[*b*][1,4]dioxin structure led to favorable effect.

Subsequently preliminary SAR (structure–activity relationship) studies were performed to deduce how the structure variation and modification could affect the anticancer activity. Firstly, a main trend was that compounds in **C** series (with IC_{50} values between 0.11 μM and 8.77 μM and GI_{50} values between 0.58 μM and 9.89 μM) showed better effect than compounds in **D** series (with IC_{50} values between 1.70 μM and 9.32 μM and GI_{50} values between 1.45 μM and 10.98 μM) while sharing the same substituent groups. However, 4 out the 15 pairs of compounds indicated an opposite situation. They were **C4** (IC_{50} = 6.55 μM; GI_{50} = 8.37 μM) and **D4** (IC_{50} = 4.01 μM; GI_{50} = 5.08 μM), **C7** (IC_{50} = 4.20 μM; GI_{50} = 5.21 μM) and **D7** (IC_{50} = 2.67 μM; GI_{50} = 3.27 μM), **C10** (IC_{50} = 1.89 μM; GI_{50} = 1.84 μM) and **D10** (IC_{50} = 1.70 μM; GI_{50} = 1.45 μM), **C13** (IC_{50} = 2.13 μM; GI_{50} = 2.50 μM) and **D13** (IC_{50} = 1.72 μM; GI_{50} = 1.49 μM). Interestingly, they all shared one similarity that there was no substituent on ring **A** but there was one on ring **B**.

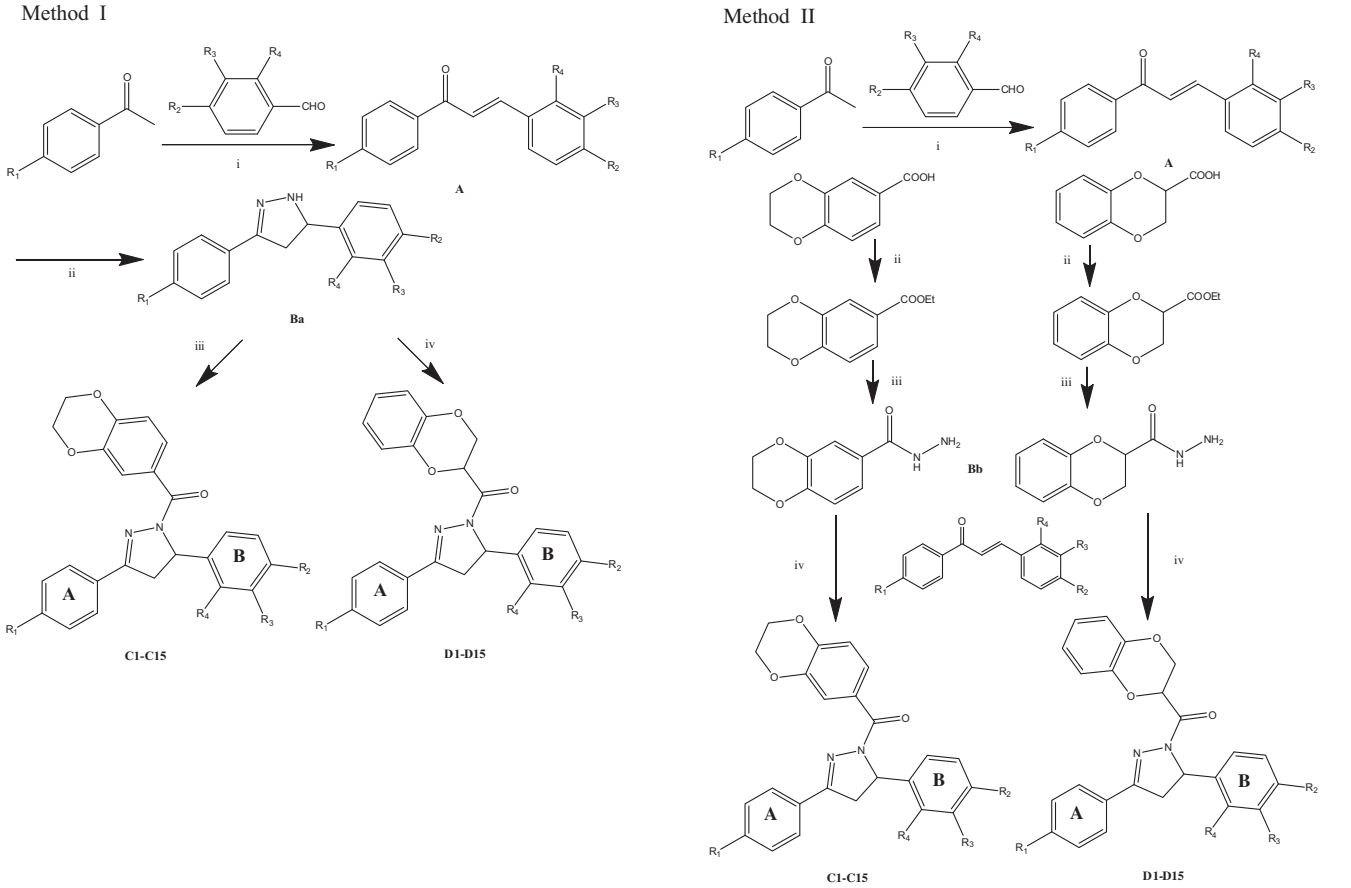

Series C	R_1	R_2	R_3	R_4	Series D	R_1	R_2	R_3	R_4
C1	H	H	H	H	D1	H	H	H	H
C2	Br	H	H	H	D2	Br	H	H	H
C3	OCH_3	H	H	H	D3	OCH_3	H	H	H
C4	H	OCH_3	H	H	D4	H	OCH_3	H	H
C5	Br	OCH_3	H	H	D5	Br	OCH_3	H	H
C6	OCH_3	OCH_3	H	H	D6	OCH_3	OCH_3	H	H
C7	H	F	H	H	D7	H	F	H	H
C8	Br	F	H	H	D8	Br	F	H	H
C9	OCH_3	F	H	H	D9	OCH_3	F	H	H
C10	H	H	F	H	D10	H	H	F	H
C11	Br	H	F	H	D11	Br	H	F	H
C12	OCH_3	H	F	H	D12	OCH_3	H	F	H
C13	H	H	H	F	D13	H	H	H	F
C14	Br	H	H	F	D14	Br	H	H	F
C15	OCH_3	H	H	F	D15	OCH_3	H	H	F

Scheme 1. General synthesis of compounds (**C1**–**C15**; **D1**–**D15**). Reagents and conditions: Method I: (i) EtOH, 40% NaOH, reflux, 30 min; (ii) EtOH, hydrazine hydrate, 80 °C, 5 h; (iii) CH_2Cl_2, 2,3-dihydrobenzo[*b*][1,4]dioxin-6-carboxylic acid, EDCI, HOBt, rt, 10 h; (iv) CH_2Cl_2, 2,3-dihydrobenzo[*b*][1,4]dioxin-2-carboxylic acid, EDCI, HOBt, rt, 10 h; Method II: (i) EtOH, 40% NaOH, reflux, 30 min; (ii) 2,3-dihydrobenzo[*b*][1,4]dioxin-6-carboxylic acid or 2,3-dihydrobenzo[*b*][1,4]dioxin-2-carboxylic acid, EtOH, 98% H_2SO_4, 80 °C, 5 h; (iii) EtOH, hydrazine, 80 °C, 5 h; (iv) EtOH, NaOH, 80 °C, 10 h.

As we can see, a strict modification was more potent and reliable in drug design while an innovative isomeric attempt did bring some pleasant surprise. Secondly, as for R_1, which is the *para*-substituent on ring **A**, we could perceive the tendency that −Br > −H ⩾ −OMe in the **C** series. For example, we could see the order that **C14** (IC_{50} = 0.11 μM; GI_{50} = 0.58 μM) > **C13** (IC_{50} = 2.13 μM; GI_{50} = 2.50 μM) ⩾ **C15** (IC_{50} = 2.97 μM; GI_{50} = 3.47 μM). However, in the **D** series, with the other factors fixed, the *para*-substituent on ring **A** indicated a trend that −H > −Br ⩾ −OMe. For example, we could perceive the order that **D7** (IC_{50} = 2.67 μM; GI_{50} = 3.27 μM) > **D8** (IC_{50} = 4.35 μM; GI_{50} = 5.63 μM) ⩾ **D9** (IC_{50} = 5.20 μM; GI_{50} = 6.19 μM). Finally, we attempted to reveal the influence of the substituent groups on ring **B**. After considering both steric and electronic complexity, we simplified the situations by locking the substituent groups on ring **A** as their optimal choice respectively. That is while analyze compounds in **C** series we fixed ring **A** with a *para*-substituted Bromine and in the analysis of **D** series we took a simple phenyl as ring **A**. In **C** series, the results of inhibitory activity inferred the order that *ortho*-Fluorine > *meta*- Fluorine > −H > *para*-Fluorine > *para*-Methoxyl. The corresponding compounds were **C14** (IC_{50} = 0.11 μM; GI_{50} = 0.58 μM) > **C11** (IC_{50} = 0.27 μM; GI_{50} = 0.81 μM) > **C2** (**IC**$_{50}$ = 1.39 μM; GI_{50} = 1.79 μM) > **C8** (IC_{50} = 2.71 μM;

Table 1
B-Raf^{V600E} inhibitory activity and anti-proliferation activity of the synthesized compounds (**C1**–**C15**, **D1**–**D15**)

Compounds	IC_{50} (μM) B-Raf^{V600E}	GI_{50}(μM) WM266.4	Compounds	IC_{50} (μM) B-Raf^{V600E}	GI_{50}(μM) WM266.4
C1	1.18 ± 0.09	1.37 ± 0.11	**D1**	3.02 ± 0.18	3.55 ± 0.40
C2	1.39 ± 0.05	1.79 ± 0.03	**D2**	5.16 ± 0.63	6.15 ± 0.82
C3	1.97 ± 0.10	2.37 ± 0.08	**D3**	5.27 ± 0.48	6.31 ± 0.59
C4	6.55 ± 0.21	8.37 ± 0.58	**D4**	4.01 ± 0.51	5.08 ± 0.44
C5	4.75 ± 0.39	5.68 ± 0.42	**D5**	7.31 ± 1.03	9.01 ± 1.21
C6	8.77 ± 0.67	9.89 ± 0.76	**D6**	9.32 ± 0.95	10.98 ± 0.99
C7	4.20 ± 0.26	5.21 ± 0.37	**D7**	2.67 ± 0.19	3.27 ± 0.34
C8	2.71 ± 0.13	3.26 ± 0.31	**D8**	4.35 ± 0.52	5.63 ± 0.68
C9	3.23 ± 0.18	3.78 ± 0.22	**D9**	5.20 ± 0.46	6.19 ± 0.70
C10	1.89 ± 0.12	1.84 ± 0.20	**D10**	1.70 ± 0.20	1.45 ± 0.15
C11	0.27 ± 0.03	0.81 ± 0.06	**D11**	5.90 ± 0.61	7.81 ± 0.73
C12	0.33 ± 0.04	0.93 ± 0.10	**D12**	5.57 ± 0.49	6.72 ± 0.77
C13	2.13 ± 0.15	2.50 ± 0.21	**D13**	1.72 ± 0.15	1.49 ± 0.12
C14	0.11 ± 0.02	0.58 ± 0.07	**D14**	6.30 ± 0.71	8.03 ± 0.86
C15	2.97 ± 0.33	3.47 ± 0.32	**D15**	4.39 ± 0.55	5.72 ± 0.47
C0	0.20 ± 0.03	0.89 ± 0.04	Erlotinib	0.06	8.12

GI_{50} = 3.26 μM) > **C5** (IC_{50} = 4.75 μM; GI_{50} = 5.68 μM). Besides, in **D** series, an observable indication was that *meta*- Fluorine > *ortho*-Fluorine > *para*-Fluorine > –H > *para*-Methoxyl. The relevant compounds were **D10** (IC_{50} = 1.70 μM; GI_{50} = 1.45 μM) > **D13** (IC_{50} = 1.72 μM; GI_{50} = 1.49 μM) > **D7** (IC_{50} = 2.67 μM; GI_{50} = 3.27 μM) > **D1** (IC_{50} = 3.02 μM; GI_{50} = 3.55 μM) > **D4** (IC_{50} = 4.01 μM; GI_{50} = 5.08 μM). A definite discipline was that *para*-Methoxyl here weakened the inhibitory activity, inferring that an electron-donating substitute with bulk size should be avoided in designing this kind of inhibitors, which exactly agreed with our previous conclusion.[18] Further, our work in this paper reveal a new inference that substituent groups on *ortho* or *meta* positions might enhance the inhibitory activity while keeping the groups electron-withdrawing and small in size. A clearer SAR analysis was expounded in the 3D-QSAR part below.

Moreover, an acute oral toxicity test was conducted with mice to determine the toxicity from a single dose via the oral route. Based on the results of study (not listed), the single dose acute oral LD_{50} (half maximal concentration of lethal does) values of the most potent compounds in their own series **C14** and **D10** are both greater than 5000 mg/kg of bodyweight.

2.3. Docking study

In molecular docking, molecular modeling techniques are used to predict how a protein (enzyme) interacts with small molecules (ligands).[23] In our present study, to explore the interactions between compounds and B-Raf and to visualize the probable binding mode, a docking study was performed using the CDocker protocol in Discovery Studio 3.1 (Discovery Studio 3.1, Accelrys, Inc. San Diego, CA). We conducted docking of our thirty 2,3-dihydrobenzo[*b*][1,4]dioxin-containing 4,5-dihydro-1*H*-pyrazole derivatives into the active site of the receptor B-Raf. We chose two crystal structures of B-Raf (PDB Code: 2FB8.pdb and 3PSD.pdb)[13,24], in which the original ligands were SB-590885 and 6-[1-(piperidin-4-yl)-3-(pyridin-4-yl)-1*H*-pyrazol-4-yl]indeno[1,2-c]pyrazole (ligand code: SM7) respectively, were obtained from the RCSB protein data bank (http://www.pdb.org). After preparing the receptor and ligands, the site sphere was selected based on the ligand binding location. Owing to the generation of random conformations conducted by the protocol as well as the similarity of the active sites, the binding models with 2FB8 and 3PSD showed the same results. The binding models of most potent compounds in two series **C14** and **D10** with 3PSD were depicted in Figures 2 and 3, respectively.

In the binding model, compound **C14** is nicely bound to 3PSD via one hydrogen bond, one π–π interaction and one π–cation interaction. One oxygen atom of 2,3-dihydrobenzo[*b*][1,4]dioxin contributes to the hydrogen bonding interaction (O···H–N: 2.02 Å, 138.991°) with the backbone amino hydrogen atom of ASP594. Meanwhile, the π–cation interaction between the benzene ring of 2,3-dihydrobenzo[*b*][1,4]dioxin and LYS483 suggests that the introduction of the heterocyclic structure has enhanced the combination of the receptor and ligand. Further, the benzene ring **B** of compound **C14** forms a π–π interaction with PHE583, which is accordant exactly with the previous work of B-Raf inhibitors.[13,18,24] As for compound **D10**, it also performs a nice bonding situation via a π–sigma interaction together with a π–cation interaction. This ensures the binding affinity and results in an increased B-Raf inhibitory activity. A remarkable π–sigma interaction is formed between the benzene ring **B** of compound **D10** and VAL471. The other is a familiar π–cation interaction with the end amino cation of LYS483 formed by the benzene ring **A**, which is distinct from **C14**. Also PHE583 has taken part in the interactions via *Van der Waals* force according to the binding model.

The receptor surface model was showed in Figure 4, which revealed that the molecules were well embedded in the active pocket including VAL471, PHE583, ALA481, THR529, LEU514 and ASN581. This active pocket is occupied by the 2,3-dihydrobenzo[*b*][1,4]dioxin structure, confirming the success of structural modification. Moreover, the docking calculation of all the compounds was also depicted in Table 2. The CDocker Interaction Energy (interaction energy between the ligand and the receptor) and the CDocker Energy (energy of the ligand–receptor complexes) agreed with the B-Raf inhibitory trend for all the synthesized compounds.

2.4. QSAR model

Part of our modification in this paper might have slightly changed the backbone of our previous inhibitors. Thus, the evaluation of the novel derivates as B-Raf inhibitors using 3D QSAR models should be rebuilt to verify the previous conclusion and to explore more potent inhibitors on a new level. By using the Create 3D QSAR protocol of Discovery Studio 3.1, all thirty compounds with definite IC_{50} values were selected as the model dataset. By convention, we use the **p IC$_{50}$** scale (−lg IC_{50}), in which higher value indicates exponentially greater potency, to measure the inhibitory activity. The training set and test set were chosen by the Diverse Molecules method in Discovery Studio 3.1. To ensure a good alignment, we chose the alignment conformation of each molecule with lowest

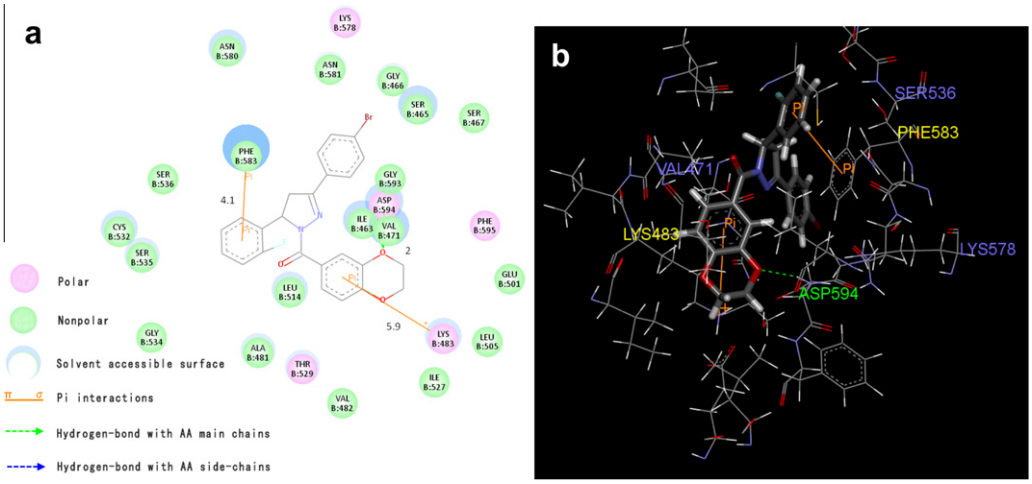

Figure 2. (a) 2D molecular docking modeling of compound **C14** with 3PSD. (b) 3D model of the interaction between compound **C14** and 3PSD bonding site. The one H-bond (green line) is displayed as dotted lines and the amino acid it acts on is labeled in green. The one π–cation interactions and one π–π interaction are shown as orange lines with their corresponding amino acids labeled in yellow. Other important amino acids are labeled in blue.

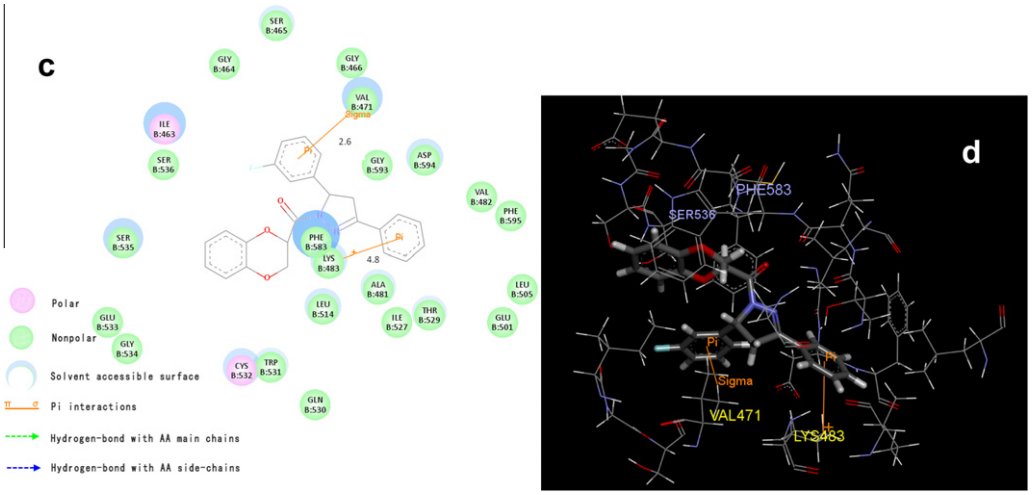

Figure 3. (c) 2D molecular docking modeling of compound **D10** with 3PSD. (d) 3D model of the interaction between compound **D10** and 3PSD bonding site. The one π–cation interaction and one π–sigma interaction are shown as orange line with their corresponding amino acid labeled in yellow. Other important amino acids are labeled in blue.

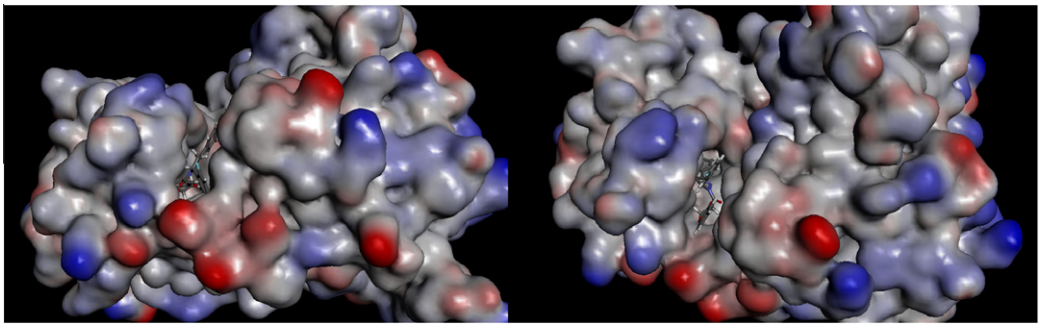

Figure 4. The receptor surface model with **C14** (left) and **D10** (right), respectively.

energy in the docked results of CDocker protocol. Besides, we applied the alignment by the substructure (4,5-dihydro-1*H*-pyrazol-1-yl)methanone before building the QSAR model.

The correlation coefficient r^2 between observed activity of testing set and training set was found to be 0.869, which proved that the QSAR model built by us is acceptable. Further, the molecules aligned with the *iso*-surfaces of the 3D QSAR model coefficients on electrostatic potential grids (Fig. 5a) and *Van der Waals* grids (Fig. 5b) are listed. Electrostatic map indicates red contours around regions where high electron density (negative charge) is expected

Table 2
The docking calculation of the synthesized compounds (**C1**–**C15**, **D1**–**D15**)

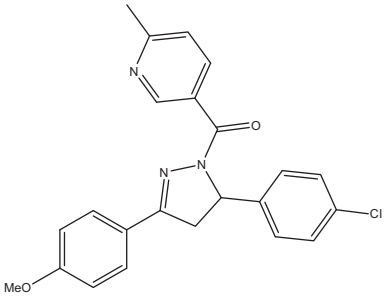

C0

Compounds	-CDocker interaction energy ΔGb (kcal/mol)	-CDocker energy ΔGb kcal/mol)	Compounds	-CDocker interaction energy ΔGb (kcal/mol)	-CDocker energy ΔGb (kcal/mol)
C1	49.9545	21.4781	**D1**	49.2347	24.9426
C2	49.8666	14.8312	**D2**	45.3963	13.4998
C3	49.7558	12.91	**D3**	45.3398	9.38154
C4	43.1425	7.55235	**D4**	46.8221	11.6309
C5	46.0606	3.86233	**D5**	40.8784	9.94429
C6	31.8095	−15.4059	**D6**	18.0335	−62.6298
C7	46.5363	15.7514	**D7**	49.4115	24.7559
C8	49.3877	13.1866	**D8**	46.2068	13.1515
C9	49.0151	8.08596	**D9**	45.3955	7.04373
C10	49.7929	20.8885	**D10**	49.832	25.2778
C11	50.5053	19.16	**D11**	44.2385	11.5947
C12	50.4033	11.5272	**D12**	45.0534	9.3477
C13	49.7242	19.6037	**D13**	49.8206	22.6055
C14	51.0408	20.4421	**D14**	43.3739	11.0938
C15	49.265	12.0063	**D15**	46.1547	9.9257
C0	40.0471	4.9598			

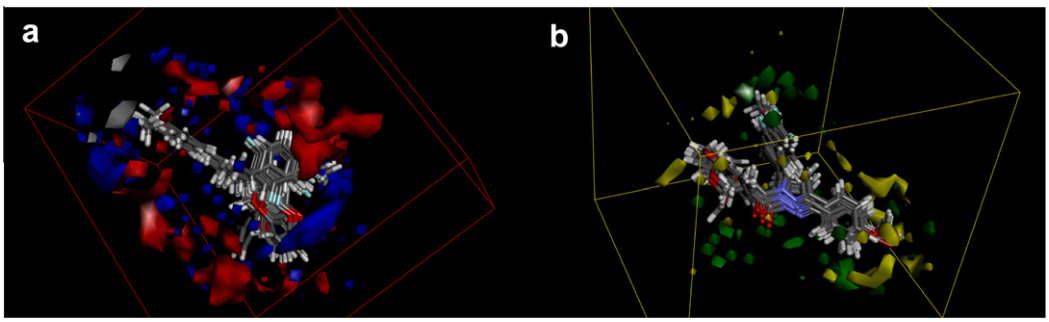

Figure 5. 3D-QSAR of 4,5-dihydro-1*H*-pyrazole derivatives containing 2,3-dihydrobenzo[*b*][1,4]dioxin moiety. Red contours mean high electron density is expected to increase activity while blue contours mean low electron density is better. Green areas mean steric bulk is better while yellow areas mean small groups are helpful.

to increase activity, and blue contours represent areas where low electron density (partial positive charge) is expected to increase activity. Similarly, steric map indicates areas where steric bulk is predicted to increase (green) or decrease (yellow) activity. According to the maps, being agreed with the fact that **C** series performed more potent activity than **D** series, a lower negative charged group with approximately the same size would help obtain sound activity. Meanwhile, on ring **A**, a lower negative charged and slightly smaller R_1 group would bring higher activity. That is a little different from our previous paper and the possible reason is the slight change of backbone caused by the introduction of heterocyclic structure. As for substituent on ring **B**, a small and high negative charged group on the *para*-position would enhance the bioactivity while a same one on the *ortho*- or/and *meta*-position might make the efficiency better. The 3D QSAR model agrees with the inhibitory activity well and provides us the direction of further modification.

3. Conclusion

To conclude, two series of compounds, **C1**–**C15** (2,3-dihydrobenzo[*b*][1,4]dioxin-6-yl)(3,5-diaryl-4,5-dihydro-1*H*-pyrazol-1-yl) methanone and **D1**–**D15** (2,3-dihydrobenzo[b][1,4]dioxin-2-yl)(3,5-diaryl-4,5-dihydro-1*H*-pyrazol-1-yl)methanone have been synthesized and evaluated for their B-Raf inhibitory and anti-proliferation activities. Compound **C14** showed the most potent biological activity against $B\text{-}Raf^{V600E}$ and WM266.4 human melanoma cell line with corresponding IC_{50} value of 0.11 μM and GI_{50} value of 0.58 μM, being comparable with the positive control and more potent than our previous best compound, while **D10** performed the best in the **D** series with corresponding IC_{50} value of 1.70 μM and GI_{50} value of 1.45 μM. The docking simulation was performed to get the probable binding models and poses. The results indicate that compounds **C14** and **D10**, which act as potential B-Raf inhibitors, can both bind well into the active site of B-Raf.

QSAR model was also built with the activity data and binding conformations to provide a reliable tool for reasonable design of B-Raf inhibitors in future. The introduction of 2,3-dihydrobenzo[*b*][1,4]dioxin structure reinforced the combination of our compounds and the receptor, resulting in progress of bioactivity.

4. Experimental section

4.1. Materials and measurements

All chemicals used were purchased from Aldrich (USA). The eluates were monitored using TLC (Thin layer chromatography). TLC was run on the silica gel coated aluminum sheets (Silica Gel 60 Å GF_{254}, E. Merk, Germany) and visualized in UV light (254 nm). Separation of the compounds by column chromatography was carried out with silica gel 60 (200–300 mesh ASTM, E. Merck, Germany). Developed plates were visualized by a Spectroline ENF 260C/F UV apparatus. The quantity of silica gel used was 50–100 times the weight charged on the column. Melting points (uncorrected) were determined on a XT4MP apparatus (Taike Corp., Beijing, China). ESI mass spectra were obtained on a Mariner System 5304 mass spectrometer, and ^{1}H NMR spectra were recorded on a DPX300 spectrometer at 25 °C with TMS and solvent signals allotted as internal standards, Chemical shifts are reported in ppm (δ). Elemental analyses were performed on a CHN-O-Rapid instrument and were within 0.4% of the theoretical values.

4.2. General method of synthesis of (E)-Chalcones (A)

Substituted acetophenone (10 mmol) and substituted benzaldehyde (10 mmol) in ethanol (25 mL) were refluxed gently for 30 min. Then 40% NaOH (5 mL) was added and the solid was filtered, washed with water and dried to obtain shiny solid **A**.

4.3. General method of synthesis of 3,5-di-substituted-phenyl-4,5-dihydro-1*H*-pyrazole (Ba)

Compound **A** 5 mmol and 80% hydrazine hydrate (5 mmol) in ethanol (20 mL) were refluxed at 80 °C for 5 h. While the reaction completed, the ethanol was evaporated. The separated solid was filtered, washed with water and dried to obtain slight yellow solid **Ba**.

4.4. General method of synthesis of 2,3-dihydrobenzo[*b*][1,4] dioxin-6-carbohydrazide and 2,3-dihydrobenzo[*b*][1,4]dioxin-6-carbohydrazide (Bb)

2,3-Dihydrobenzo[*b*][1,4]dioxin-6-carboxylic acid (or 2,3-dihydrobenzo[*b*][1,4]dioxin-2-carboxylic acid) (1 mmol) and 98% H_2SO_4 (1 ml) in ethanol (20 mL) were refluxed at 80 °C for 5 h. While the reaction completed, 80% hydrazine hydrate (2 mmol) was added and then the solution was refluxed at 80 °C for another 5 h. While the reaction completed, the ethanol was evaporated. The separated solid was filtered, washed with cold ethanol and dried to obtain white solid **Bb**.

4.5. General method of synthesis of (2,3-dihydrobenzo[*b*][1,4] dioxin-6-yl)(3,5-diaryl-4,5-dihydro-1*H*-pyrazol-1-yl)methanone (C1–C15) and (2,3-dihydrobenzo[*b*][1,4]dioxin-2-yl)(3,5-diaryl-4,5-dihydro-1*H*-pyrazol-1-yl)methanone (D1–D15)

Method I **Ba** (1 mmol) and 2,3-dihydrobenzo[*b*][1,4]dioxin-6-carboxylic acid (or 2,3-dihydrobenzo[*b*][1,4]dioxin-2-carboxylic acid) (1 mmol) together with EDCI (1.5 mmol) and HOBt (0.05 mmol) in CH_2Cl_2 (20 mL) were refluxed at room temperature for 10 h. While the reaction completed, the solution was washed with water for three times (30 mL each time). The remaining water layer was extracted by EtOAc for three times (30 mL each time). The organic layers (CH_2Cl_2 and EtOAc) were combined and then evaporated. The separated solid was crystallized from mixture of DMF and ethanol (9:1) to obtain the corresponding compound as translucent solid.

Method II **Bb** (1 mmol) and **A** (1 mmol) in ethanol (20 mL) were refluxed at 80 °C for 5 h with NaOH (0.05 mmol). Then the product was obtained through a column chromatography with mixed eluent (V_{EtOAc}:$V_{Petroleum\ ether}$ = 5:1). The solvent was evaporated and the separated solid was crystallized from mixture of DMF and ethanol (9:1) to obtain the corresponding compound as translucent solid.

4.5.1. (2,3-dihydrobenzo[*b*][1,4]dioxin-6-yl)(3,5-diphenyl-4,5-dihydro-1*H*-pyrazol-1-yl)methanone (C1)

White crystal, mp: 120–121 °C. ^{1}H NMR ($CDCl_3$, 300 MHz) δ: 3.15–3.23 (d, J = 17.7 Hz, 1H), 3.69–3.79 (m, 1H), 4.31–4.32 (t, J = 2.4 Hz, 4H), 5.79–5.85 (m, 1H), 6.90–6.93 (d, J = 8.4 Hz, 1H), 7.27–7.37 (m, 5H), 7.43–7.44 (m, 3H), 7.65–7.68 (d, J = 8.1 Hz, 2H), 7.73–7.75 (m, 2H). MS (ESI): 385.15 ($C_{24}H_{21}N_2O_3$, $[M+H]^+$). Anal. Calcd for $C_{24}H_{20}N_2O_3$: C, 74.98; H, 5.24; N, 7.29; O, 12.49. Found: C, 74.59; H, 5.23; N, 7.30.

4.5.2. (3-(4-Bromophenyl)-5-phenyl-4,5-dihydro-1*H*-pyrazol-1-yl)(2,3-dihydrobenzo[*b*][1,4]dioxin-6-yl)methanone (C2)

Yellow crystal, mp: 189–190 °C. ^{1}H NMR ($CDCl_3$, 300 MHz) δ: 3.12–3.17 (d, J = 10.5 Hz, 1H), 3.70–3.77 (m, 1H), 4.29–4.34 (t, J = 4.5 Hz, 4H), 5.79–5.82 (m, 1H), 6.90–6.95 (d, J = 11.7 Hz, 2H), 7.29–7.42 (m, 3H), 7.53–7.59 (m, 4H), 7.65–7.67 (m, 3H). MS (ESI): 463.06 ($C_{24}H_{20}BrN_2O_3$, $[M+H]^+$). Anal. Calcd for $C_{24}H_{19}BrN_2O_3$: C, 62.22; H, 4.13; Br, 17.25; N, 6.05; O, 10.36. Found: C, 62.07; H, 4.12; N, 6.06.

4.5.3. (2,3-Dihydrobenzo[*b*][1,4]dioxin-6-yl)(3-(4-methoxyphenyl)-5-phenyl-4,5-dihydro-1*H*-pyrazol-1-yl)methanone (C3)

White crystal, mp: 199–200 °C. ^{1}H NMR ($CDCl_3$, 300 MHz) δ: 3.70–3.80 (m, 2H), 3.84 (s, 3H), 4.28–4.30 (m, 4H), 5.77–5.80 (m, 1H), 6.89–6.94 (m, 3H), 7.24–7.26 (m, 1H), 7.31–7.32 (d, 4H, J = 2.1 Hz), 7.64–7.72 (m, 4H). MS (ESI): 415.16 ($C_{25}H_{23}N_2O_4$, $[M+H]^+$). Anal. Calcd for $C_{25}H_{22}N_2O_4$: C, 72.45; H, 5.35; N, 6.76; O, 15.44. Found: C, 72.11; H, 5.33; N, 6.77.

4.5.4. (2,3-Dihydrobenzo[*b*][1,4]dioxin-6-yl)(5-(4-methoxyphenyl)-3-phenyl-4,5-dihydro-1*H*-pyrazol-1-yl)methanone (C4)

White crystal, mp: 123–124 °C. ^{1}H NMR ($CDCl_3$, 300 MHz) δ: 3.15–3.22 (d, J = 17.1 Hz, 1H), 3.72–3.78 (m, 1H), 3.81 (s, 3H), 4.31–4.32 (t, J = 2.4 Hz, 4H), 5.75–5.80 (m, 1H), 6.85–6.92 (m, 3H), 7.24–7.26 (m, 2H), 7.42–7.44 (m, 3H), 7.64–7.66 (d, J = 7.8 Hz, 2H), 7.73–7.76 (m, 2H). MS (ESI): 415.16 ($C_{25}H_{23}N_2O_4$, $[M+H]^+$). Anal. Calcd for $C_{25}H_{22}N_2O_4$: C, 72.45; H, 5.35; N, 6.76; O, 15.44. Found: C, 72.21; H, 5.34; N, 6.76.

4.5.5. (3-(4-Bromophenyl)-5-(4-methoxyphenyl)-4,5-dihydro-1*H*-pyrazol-1-yl)(2,3-dihydrobenzo[*b*][1,4]dioxin-6-yl)methanone (C5)

Yellow crystal, mp: 205–207 °C. ^{1}H NMR ($CDCl_3$, 300 MHz) δ: 3.16–3.24 (d, J = 16.2 Hz, 1H), 3.75–3.80 (m, 1H), 3.83 (s, 3H), 4.33–4.34 (t, 4H, J = 2.4 Hz, 4H), 5.77–5.81 (m, 1H), 6.86–6.93 (m, 3H), 7.25–7.28 (m, 2H), 7.43–7.47 (m, 1H), 7.55 (s, 1H), 7.70–7.73 (d, J = 8.1 Hz, 2H), 7.78–7.81 (m, 2H). MS (ESI): 493.07 ($C_{25}H_{22}BrN_2O_4$, $[M+H]^+$). Anal. Calcd for $C_{25}H_{21}BrN_2O_4$: C, 60.86;

H, 4.29; Br, 16.20; N, 5.68; O, 12.97. Found: C, 60.59; H, 4.27; N, 5.70.

4.5.6. (3,5-Bis(4-methoxyphenyl)-4,5-dihydro-1*H*-pyrazol-1-yl)(2,3-dihydrobenzo[*b*][1,4]dioxin-6-yl)methanone (C6)

White crystal, mp: 144–146 °C. ^{1}H NMR ($CDCl_3$, 300 MHz) δ: 3.12–3.18 (d, J = 16.8 Hz, 1H), 3.69–3.76 (m, 1H), 3.82 (s, 6H), 4.31–4.33 (t, J = 2.4 Hz, 4H), 5.72–5.77 (m, 1H), 6.83–6.90 (m, 3H), 7.19–7.23 (m, 2H), 7.43–7.46 (m, 1H), 7.59 (s, 1H), 7.71–7.74 (d, J = 8.1 Hz, 2H), 7.82–7.84 (d, J = 7.2 Hz, 2H). MS (ESI): 445.17 ($C_{26}H_{25}N_2O_5$, $[M+H]^+$). Anal. Calcd for $C_{26}H_{24}N_2O_5$: C, 70.26; H, 5.44; N, 6.30; O, 18.00. Found: C, 69.97; H, 5.44; N, 6.32.

4.5.7. (2,3-Dihydrobenzo[*b*][1,4]dioxin-6-yl)(5-(4-fluorophenyl)-3-phenyl-4,5-dihydro-1*H*-pyrazol-1-yl)methanone (C7)

White crystal, mp: 137–138 °C. ^{1}H NMR ($CDCl_3$, 300 MHz) δ: 3.20–3.26 (d, J = 17.4 Hz, 1H), 3.76–3.81 (m, 1H), 4.33–4.34 (t, J = 2.1 Hz, 4H), 5.76–5.82 (m, 1H), 7.05–7.12 (m, 3H), 7.25–7.28 (m, 2H), 7.45–7.51 (m, 4H), 7.59 (s, 1H), 7.65–7.68 (d, J = 8.1 Hz, 2H). MS (ESI): 403.14 ($C_{24}H_{20}FN_2O_3$, $[M+H]^+$). Anal. Calcd for $C_{24}H_{19}FN_2O_3$: C, 71.63; H, 4.76; F, 4.72; N, 6.96; O, 11.93. Found: C, 71.31; H, 4.75; N, 6.97.

4.5.8. (3-(4-Bromophenyl)-5-(4-fluorophenyl)-4,5-dihydro-1*H*-pyrazol-1-yl)(2,3-dihydrobenzo[*b*][1,4]dioxin-6-yl)methanone (C8)

Yellow crystal, mp: 226–229 °C. ^{1}H NMR ($CDCl_3$, 300 MHz) δ: 3.19–3.24 (d, J = 16.2 Hz, 1H), 3.74–3.79 (m, 1H), 4.32–4.33 (t, J = 3.0 Hz, 4H), 5.69–5.75 (m, 1H), 7.02–7.10 (m, 3H), 7.23–7.25 (m, 2H), 7.47–7.54 (m, 3H), 7.60 (s, 1H), 7.68–7.71 (d, J = 7.8 Hz, 2H). MS (ESI): 481.05 ($C_{24}H_{19}BrFN_2O_3$, $[M+H]^+$). Anal. Calcd for $C_{24}H_{18}BrFN_2O_3$: C, 59.89; H, 3.77; Br, 16.60; F, 3.95; N, 5.82; O, 9.97. Found: C, 59.66; H, 3.75; N, 5.83.

4.5.9. (2,3-Dihydrobenzo[*b*][1,4]dioxin-6-yl)(5-(4-fluorophenyl)-3-(4-methoxyphenyl)-4,5-dihydro-1*H*-pyrazol-1-yl)methanone (C9)

White crystal, yield mp: 236–237 °C. ^{1}H NMR ($CDCl_3$, 300 MHz) δ: 3.18–3.23(d, J = 16.8 Hz, 1H), 3.72–3.78 (m, 1H), 3.82 (s, 3H), 4.31–4.32 (t, J = 2.7 Hz, 4H), 5.72–5.78 (m, 1H), 7.04–7.11 (m, 5H), 7.22–7.25 (m, 2H), 7.43–7.49 (m, 1H), 7.58 (s, 1H), 7.74–7.76 (d, J = 7.2 Hz, 2H). MS (ESI): 433.15 ($C_{25}H_{22}FN_2O_4$, $[M+H]^+$). Anal. Calcd for $C_{25}H_{21}FN_2O_4$: C, 69.44; H, 4.89; F, 4.39; N, 6.48; O, 14.80. Found: C, 69.08; H, 4.86; N, 6.49.

4.5.10. (2,3-Dihydrobenzo[*b*][1,4]dioxin-6-yl)(5-(3-fluorophenyl)-3-phenyl-4,5-dihydro-1*H*-pyrazol-1-yl)methanone (C10)

White crystal, mp: 105–107 °C. ^{1}H NMR ($CDCl_3$, 300 MHz) δ: 3.19–3.24 (d, J = 16.2 Hz, 1H), 3.65–3.73 (m, 1H), 4.32 (t, J = 2.1 Hz, 4H), 5.72–5.78 (m, 1H), 6.78 (s, 1H), 6.95–7.09 (m, 3H), 7.23–7.26 (m, 1H), 7.44–7.53 (m, 4H), 7.57 (s, 1H), 7.62–7.65 (d, J = 8.4 Hz, 2H). MS (ESI): 403.14 ($C_{24}H_{20}FN_2O_3$, $[M+H]^+$). Anal. Calcd for $C_{24}H_{19}FN_2O_3$: C, 71.63; H, 4.76; F, 4.72; N, 6.96; O, 11.93. Found: C, 71.37; H, 4.74; N, 6.98.

4.5.11. (3-(4-Bromophenyl)-5-(3-fluorophenyl)-4,5-dihydro-1*H*-pyrazol-1-yl)(2,3-dihydrobenzo[*b*][1,4]dioxin-6-yl)methanone (C11)

Yellow crystal, mp: 135–137 °C. ^{1}H NMR ($CDCl_3$, 300 MHz) δ: 3.22–3.27 (d, J = 16.5 Hz, 1H), 3.77–3.82 (m, 1H), 4.34 (t, J = 2.1 Hz, 4H), 5.70–5.76 (m, 1H), 6.79 (s, 1H), 6.91–7.05 (m, 3H), 7.31–7.33 (m, 1H), 7.49–7.57 (m, 3H), 7.61 (s, 1H), 7.68–7.71 (d, J = 7.5 Hz, 2H). MS (ESI): 481.05 ($C_{24}H_{19}BrFN_2O_3$, $[M+H]^+$). Anal. Calcd for $C_{24}H_{18}BrFN_2O_3$: C, 59.89; H, 3.77; Br, 16.60; F, 3.95; N, 5.82; O, 9.97. Found: C, 59.52; H, 3.74; N, 5.82.

4.5.12. (2,3-Dihydrobenzo[*b*][1,4]dioxin-6-yl)(5-(3-fluorophenyl)-3-(4-methoxyphenyl)-4,5-dihydro-1*H*-pyrazol-1-yl)methanone (C12)

White crystal, mp: 162–163 °C. ^{1}H NMR ($CDCl_3$, 300 MHz) δ: 3.11–3.17 (m, 1H), 3.70–3.80 (m, 1H), 3.86 (s, 3H), 4.32–4.37 (t, J = 5.4 Hz, 4H), 5.76–5.82 (m, 1H), 6.91–6.98 (m, 4H), 7.03 (s, 1H), 7.10–7.13 (d, J = 7.8 Hz, 1H), 7.66–7.70 (m, 4H), 7.74 (s, 1H). MS (ESI): 433.15 ($C_{25}H_{22}FN2O_4$, $[M+H]^+$). Anal. Calcd for $C_{25}H_{21}FN2O_4$: C, 69.44; H, 4.89; F, 4.39; N, 6.48; O, 14.80. Found: C, 69.16; H, 4.87; N, 6.49.

4.5.13. (2,3-Dihydrobenzo[*b*][1,4]dioxin-6-yl)(5-(2-fluorophenyl)-3-phenyl-4,5-dihydro-1*H*-pyrazol-1-yl)methanone (C13)

White crystal, mp: 176–177 °C. ^{1}H NMR ($CDCl_3$, 300 MHz) δ: 3.20–3.27 (m, 1H), 3.81–3.86 (m, 1H), 4.39–4.41 (t, J = 4.2 Hz, 4H), 5.62–5.69 (m, 1H), 6.91–6.99 (m, 2H), 7.21–7.24 (d, J = 9.0 Hz, 1H), 7.43–7.46 (m, 3H), 7.50–7.54 (m, 3H), 7.60 (s, 1H), 7.71–7.74 (d, J = 7.8 Hz, 2H). MS (ESI): 403.14 ($C_{24}H_{20}FN_2O_3$, $[M+H]^+$). Anal. Calcd for $C_{24}H_{19}FN_2O_3$: C, 71.63; H, 4.76; F, 4.72; N, 6.96; O, 11.93. Found: C, 71.35; H, 4.75; N, 7.00.

4.5.14. (3-(4-Bromophenyl)-5-(2-fluorophenyl)-4,5-dihydro-1*H*-pyrazol-1-yl)(2,3-dihydrobenzo[*b*][1,4]dioxin-6-yl)methanone (C14)

White crystal, mp: 140–141 °C. ^{1}H NMR ($CDCl_3$, 300 MHz) δ: 3.23–3.29 (d, J = 17.1 Hz, 1H), 3.80–3.87 (m, 1H), 4.35–4.37 (t, J = 3.9 Hz, 4H), 5.63–5.69 (m, 1H), 6.90–6.96 (m, 2H), 7.11 (m, 1H), 7.33–7.35 (d, J = 6.6 Hz, 1H), 7.47–7.50 (m, 4H), 7.59 (s, 1H), 7.66–7.69 (d, J = 8.4 Hz, 2H). MS (ESI): 481.05 ($C_{24}H_{19}BrFN_2O_3$, $[M+H]^+$). Anal. Calcd for $C_{24}H_{18}BrFN_2O_3$: C, 59.89; H, 3.77; Br, 16.60; F, 3.95; N, 5.82; O, 9.97. Found: C, 59.72; H, 3.74; N, 5.82.

4.5.15. (2,3-Dihydrobenzo[*b*][1,4]dioxin-6-yl)(5-(2-fluorophenyl)-3-(4-methoxyphenyl)-4,5-dihydro-1*H*-pyrazol-1-yl)methanone (C15)

White crystal, mp: 173–175 °C. ^{1}H NMR ($CDCl_3$, 300 MHz) δ: 3.18–3.24 (d, J = 16.8 Hz, 1H), 3.71–3.81 (m, 1H), 3.85 (s, 3H), 4.49–4.51 (t, J = 5.1 Hz, 4H), 5.67–5.69 (m, 1H), 6.91–6.99 (m, 4H), 7.07–7.11 (d, J = 8.7 Hz, 1H), 7.42–7.47 (m, 3H), 7.59 (s, 1H), 7.75–7.78 (d, J = 8.7 Hz, 2H). MS (ESI): 433.15 ($C_{25}H_{22}FN_2O_4$, $[M+H]^+$). Anal. Calcd for $C_{25}H_{21}FN_2O_4$: C, 69.44; H, 4.89; F, 4.39; N, 6.48; O, 14.80. Found: C, 69.01; H, 4.86; N, 6.48.

4.5.16. (2,3-Dihydrobenzo[*b*][1,4]dioxin-2-yl)(3,5-diphenyl-4,5-dihydro-1*H*-pyrazol-1-yl)methanone (D1)

White crystal, mp: 201 °C. ^{1}H NMR ($CDCl_3$, 300 MHz) δ: 3.21–3.27 (m, 1H), 3.79–3.83 (m, 1H), 4.38–4.46 (m, 1H), 4.53–4.63 (m, 1H), 5.59–5.66 (m, 2H), 6.82–6.88 (m, 3H), 6.99–7.00 (d, J = 4.8 Hz, 1H), 7.21–7.26 (m, 3H), 7.30–7.34 (m, 2H), 7.44–7.48 (m, 3H), 7.75–7.76 (d, J = 3.9 Hz, 2H). MS (ESI): 385.15 ($C_{24}H_{21}N_2O_3$, $[M+H]^+$). Anal. Calcd for $C_{24}H_{20}N_2O_3$: C, 74.98; H, 5.24; N, 7.29; O, 12.49. Found: C, 74.61; H, 5.23; N, 7.31.

4.5.17. (3-(4-Bromophenyl)-5-phenyl-4,5-dihydro-1*H*-pyrazol-1-yl)(2,3-dihydrobenzo[*b*][1,4]dioxin-2-yl)methanone (D2)

Yellow crystal, mp: 233–235 °C. ^{1}H NMR ($CDCl_3$, 300 MHz) δ: 3.16–3.23 (d, J = 10.2 Hz, 1H), 3.75–3.82 (m, 1H), 4.35–4.45 (m, 1H), 4.52–4.61 (m, 1H), 5.57–5.63 (m, 2H), 6.92–6.97 (d, J = 10.8 Hz, 2H), 7.31–7.44 (m, 4H), 7.57–7.62 (m, 4H), 7.69–7.72 (m, 3H). MS (ESI): 463.06 ($C_{24}H_{20}BrN_2O_3$, $[M+H]^+$). Anal. Calcd for $C_{24}H_{19}BrN_2O_3$: C, 62.22; H, 4.13; Br, 17.25; N, 6.05; O, 10.36. Found: C, 61.93; H, 4.11; N, 6.05.

4.5.18. (2,3-Dihydrobenzo[*b*][1,4]dioxin-2-yl)(3-(4-methoxyphenyl)-5-phenyl-4,5-dihydro-1*H*-pyrazol-1-yl)methanone (D3)

White crystal, mp: 223–225 °C. ^{1}H NMR ($CDCl_3$, 300 MHz) δ: 3.20–3.24 (d, J = 10.2 Hz, 1H), 3.71–3.80 (m, 1H), 3.87 (s, 3H), 4.42–4.45 (m, 1H), 4.51–4.54 (d, J = 6.9 Hz, 1H), 5.57–5.60 (m, 1H), 5.62–5.63 (m, 1H), 6.82–6.89 (m, 3H), 6.95–6.97 (d, J = 5.1 Hz, 2H), 7.00–7.02 (d, J = 5.4 Hz, 1H), 7.22–7.26 (m, 3H), 7.30–7.33 (m, 2H), 7.69–7.71 (d, J = 5.4 Hz, 2H). MS (ESI): 415.16 ($C_{25}H_{23}N_2O_4$, $[M+H]^+$). Anal. Calcd for $C_{25}H_{22}N_2O_4$: C, 72.45; H, 5.35; N, 6.76; O, 15.44. Found: C, 72.18; H, 5.34; N, 6.79.

4.5.19. (2,3-Dihydrobenzo[*b*][1,4]dioxin-2-yl)(5-(4-methoxyphenyl)-3-phenyl-4,5-dihydro-1*H*-pyrazol-1-yl)methanone (D4)

White crystal, mp: 104–106 °C. ^{1}H NMR ($CDCl_3$, 300 MHz) δ: 3.18–3.25 (d, J = 17.7 Hz, 1H), 3.68–3.75 (m, 1H), 3.77 (s, 3H), 4.33–4.39 (m, 1H), 4.57–4.62 (d, J = 11.4 Hz, 1H), 5.55–5.58 (m, 2H), 6.82–6.86 (m, 5H), 6.99–7.02 (m, 1H), 7.14–7.17 (d, J = 8.7 Hz, 2H), 7.43–7.46 (m, 3H), 7.73–7.77 (d, J = 7.5 Hz, 2H). MS (ESI): 415.16 ($C_{25}H_{23}N_2O_4$, $[M+H]^+$). Anal. Calcd for $C_{25}H_{22}N_2O_4$: C, 72.45; H, 5.35; N, 6.76; O, 15.44. Found: C, 72.05; H, 5.34; N, 6.78.

4.5.20. (3-(4-Bromophenyl)-5-(4-methoxyphenyl)-4,5-dihydro-1*H*-pyrazol-1-yl)(2,3-dihydrobenzo[*b*][1,4]dioxin-2-yl)methanone (D5)

Yellow crystal, mp: 198–201 °C. ^{1}H NMR ($CDCl_3$, 300 MHz) δ: 3.17–3.24 (d, J = 17.4 Hz, 1H), 3.67–3.75 (m, 1H), 3.80 (s, 3H), 4.32–4.37 (m, 1H), 4.58–4.62 (d, J = 10.8 Hz, 1H), 5.54–5.58 (m, 2H), 6.82–6.90 (m, 6H), 7.12–7.15 (d, J = 9.0 Hz, 2H), 7.49–7.52 (d, J = 8.1 Hz, 2H), 7.77–7.80 (d, J = 7.8 Hz, 2H). MS (ESI): 493.07 ($C_{25}H_{22}BrN_2O_4$, $[M+H]^+$). Anal. Calcd for $C_{25}H_{21}BrN_2O_4$: C, 60.86; H, 4.29; Br, 16.20; N, 5.68; O, 12.97. Found: C, 60.68; H, 4.28; N, 5.71.

4.5.21. (3,5-Bis(4-methoxyphenyl)-4,5-dihydro-1*H*-pyrazol-1-yl)(2,3-dihydrobenzo[*b*][1,4]dioxin-2-yl)methanone (D6)

White crystal, mp: 171–172 °C. ^{1}H NMR ($CDCl_3$, 300 MHz) δ: 3.19–3.25 (d, J = 17.7 Hz, 1H), 3.69–3.78 (m, 1H), 3.81 (s, 6H), 4.33–4.39 (m, 1H), 4.56–4.60 (d, J = 10.1 Hz, 1H), 5.53–5.56 (m, 2H), 6.81–6.83 (d, J = 7.2 Hz, 2H), 6.89–6.93 (m, 4H), 7.14–7.16 (d, J = 8.7 Hz, 2H), 7.43–7.46 (d, J = 8.1 Hz, 2H), 7.78–7.80 (d, J = 7.8 Hz, 2H). MS (ESI): 445.17 ($C_{26}H_{25}N_2O_5$, $[M+H]^+$). Anal. Calcd for $C_{26}H_{24}N_2O_5$: C, 70.26; H, 5.44; N, 6.30; O, 18.00. Found: C, 69.87; H, 5.44; N, 6.33.

4.5.22. (2,3-Dihydrobenzo[*b*][1,4]dioxin-2-yl)(5-(4-fluorophenyl)-3-phenyl-4,5-dihydro-1*H*-pyrazol-1-yl)methanone (D7)

White crystal, mp: 159–161 °C. ^{1}H NMR ($CDCl_3$, 300 MHz) δ: 3.15–3.21 (d, J = 16.8 Hz, 1H), 3.70–3.74 (m, 1H), 4.32–4.37 (m, 1H), 4.53–4.57 (d, J = 11.1 Hz, 1H), 5.53–5.57 (m, 2H), 6.81–6.87 (m, 4H), 6.97–7.03 (m, 2H), 7.12–7.15 (d, J = 9.0 Hz, 2H), 7.44–7.47 (m, 3H), 7.71–7.74 (d, J = 7.2 Hz, 2H). MS (ESI): 403.14 ($C_{24}H_{20}FN_2O_3$, $[M+H]^+$). Anal. Calcd for $C_{24}H_{19}FN_2O_3$: C, 71.63; H, 4.76; F, 4.72; N, 6.96; O, 11.93. Found: C, 71.24; H, 4.76; N, 6.98.

4.5.23. (3-(4-Bromophenyl)-5-(4-fluorophenyl)-4,5-dihydro-1*H*-pyrazol-1-yl)(2,3-dihydrobenzo[*b*][1,4]dioxin-2-yl)methanone (D8)

Yellow crystal, mp: 233–234 °C. ^{1}H NMR ($CDCl_3$, 300 MHz) δ: 3.15–3.21 (m, 1H), 3.69–3.78 (m, 1H), 4.35–4.39 (m, 1H), 4.55–4.59 (d, J = 11.1 Hz, 1H), 5.55–5.58 (m, 2H), 6.83–6.89 (m, 4H), 6.99–7.05 (m, 2H), 7.13–7.16 (d, J = 8.4 Hz, 2H), 7.45–7.48 (d, J = 7.8 Hz, 2H), 7.68–7.71 (d, J = 7.5 Hz, 2H). MS (ESI): 481.05 ($C_{24}H_{19}BrFN_2O_3$, $[M+H]^+$). Anal. Calcd for $C_{24}H_{18}BrFN_2O_3$: C, 59.89; H, 3.77; Br, 16.60; F, 3.95; N, 5.82; O, 9.97. Found: C, 59.71; H, 3.76; N, 5.85.

4.5.24. (2,3-Dihydrobenzo[*b*][1,4]dioxin-2-yl)(5-(4-fluorophenyl)-3-(4-methoxyphenyl)-4,5-dihydro-1*H*-pyrazol-1-yl)methanone (D9)

White crystal, mp: 229–231 °C. ^{1}H NMR ($CDCl_3$, 300 MHz) δ: 3.18–3.24 (d, J = 17.1 Hz, 1H), 3.71–3.76 (m, 1H), 3.81 (s, 3H), 4.32–4.36 (m, 1H), 4.54–4.57 (m, 1H), 5.60–5.64 (m, 2H), 6.88–6.94 (m, 4H), 7.01–7.07 (m, 2H), 7.16–7.19 (d, J = 8.7 Hz, 2H), 7.29–7.31 (d, J = 7.5 Hz, 2H), 7.72–7.74 (d, J = 7.2 Hz, 2H). MS (ESI): 433.15 ($C_{25}H_{22}FN_2O_4$, $[M+H]^+$). Anal. Calcd for $C_{25}H_{21}FN_2O_4$: C, 69.44; H, 4.89; F, 4.39; N, 6.48; O, 14.80. Found: C, 69.15; H, 4.86; N, 6.51.

4.5.25. (2,3-Dihydrobenzo[*b*][1,4]dioxin-2-yl)(5-(3-fluorophenyl)-3-phenyl-4,5-dihydro-1*H*-pyrazol-1-yl)methanone (D10)

White crystal, mp: 118–119 °C. ^{1}H NMR ($CDCl_3$, 300 MHz) δ: 3.13–3.20 (d, J = 17.7 Hz, 1H), 3.62–3.71 (m, 1H), 4.30–4.33 (m, 1H), 4.55–4.58 (m, 1H), 5.66–5.71 (m, 2H), 6.77 (s, 1H), 6.89–7.02 (m, 4H), 7.08–7,13 (m, 2H), 7.31–7.35 (m, 1H), 7.46–7.54 (m, 3H), 7.61–7.64 (d, J = 7.8 Hz, 2H). MS (ESI): 403.14 ($C_{24}H_{20}FN_2O_3$, $[M+H]^+$). Anal. Calcd for $C_{24}H_{19}FN_2O_3$: C, 71.63; H, 4.76; F, 4.72; N, 6.96; O, 11.93. Found: C, 71.25; H, 4.75; N, 6.99.

4.5.26. (3-(4-Bromophenyl)-5-(3-fluorophenyl)-4,5-dihydro-1*H*-pyrazol-1-yl)(2,3-dihydrobenzo[*b*][1,4]dioxin-2-yl)methanone (D11)

Yellow crystal, mp: 143–144 °C. ^{1}H NMR ($CDCl_3$, 300 MHz) δ: 3.14–3.20 (d, J = 17.1 Hz, 1H), 3.73–3.78 (m, 1H), 4.35 (m, 1H), 4.56–4.59 (d, J = 10.8 Hz, 1H), 5.68–5.72 (m, 2H), 6.77 (s, 1H), 6.88–7.03 (m, 6H), 7.29–7.31 (m, 1H), 7.50–7.53 (d, J = 8.1 Hz, 2H), 7.67–7.70 (d, J = 7.2 Hz, 2H). MS (ESI): 481.05 ($C_{24}H_{19}BrFN_2O_3$, $[M+H]^+$). Anal. Calcd for $C_{24}H_{18}BrFN_2O_3$: C, 59.89; H, 3.77; Br, 16.60; F, 3.95; N, 5.82; O, 9.97. Found: C, 59.71; H, 3.76; N, 5.85.

4.5.27. (2,3-Dihydrobenzo[*b*][1,4]dioxin-2-yl)(5-(3-fluorophenyl)-3-(4-methoxyphenyl)-4,5-dihydro-1*H*-pyrazol-1-yl)methanone (D12)

White crystal, mp: 174–176 °C. ^{1}H NMR ($CDCl_3$, 300 MHz) δ: 3.12–3.17 (m, 1H), 3.68–3.79 (m, 1H), 3.84 (s, 3H), 4.31–4.35 (m, 1H), 4.54–4.58 (m, 1H), 5.75–5.81 (m, 2H), 6.88–6.96 (m, 4H), 7.01 (s, 1H), 7.07–7.11 (m, 4H), 7.46–7.50 (m, 1H), 7.75–7.78 (d, J = 7.5 Hz, 2H). MS (ESI): 433.15 ($C_{25}H_{22}FN2O_4$, $[M+H]^+$). Anal. Calcd for $C_{25}H_{21}FN2O_4$: C, 69.44; H, 4.89; F, 4.39; N, 6.48; O, 14.80. Found: C, 69.05; H, 4.88; N, 6.50.

4.5.28. (2,3-Dihydrobenzo[*b*][1,4]dioxin-2-yl)(5-(2-fluorophenyl)-3-phenyl-4,5-dihydro-1*H*-pyrazol-1-yl)methanone (D13)

White crystal, mp: 189–190 °C. ^{1}H NMR ($CDCl_3$, 300 MHz) δ: 3.22–3.29 (m, 1H), 3.83–3.89 (m, 1H), 4.43–4.51 (m, 1H), 4.53–4.67 (m, 1H), 5.60–5.68 (m, 1H), 5.80–5.85 (m, 1H), 6.86–6.90 (m, 3H), 7.02–7.17 (m, 3H), 7.21–7.26 (m, 2H), 7.45–7.48 (m, 3H), 7.75–7.78 (d, J = 7.8 Hz, 2H). MS (ESI): 403.14 ($C_{24}H_{20}FN_2O_3$, $[M+H]^+$). Anal. Calcd for $C_{24}H_{19}FN_2O_3$: C, 71.63; H, 4.76; F, 4.72; N, 6.96; O, 11.93. Found: C, 71.25; H, 4.73; N, 6.97.

4.5.29. (3-(4-Bromophenyl)-5-(2-fluorophenyl)-4,5-dihydro-1*H*-pyrazol-1-yl)(2,3-dihydrobenzo[*b*][1,4]dioxin-2-yl)methanone (D14)

White crystal, mp: 199–201 °C. ^{1}H NMR ($CDCl_3$, 300 MHz) δ: 3.21–3.27 (m, 1H), 3.82–3.88 (m, 1H), 4.45–4.66 (m, 2H), 5.61–5.66 (m, 1H), 5.80–5.84 (m, 1H), 6.86–6.88 (m, 3H), 7.02–7.23

(m, 4H), 7.47 (m, 3H), 7.74–7.77 (d, J = 7.5 Hz, 2H). MS (ESI): 481.05 ($C_{24}H_{19}BrFN_2O_3$, $[M+H]^+$). Anal. Calcd for $C_{24}H_{18}BrFN_2O_3$: C, 59.89; H, 3.77; Br, 16.60; F, 3.95; N, 5.82; O, 9.97. Found: C, 59.72; H, 3.75; N, 5.83.

4.5.30. (2,3-Dihydrobenzo[*b*][1,4]dioxin-2-yl)(5-(2-fluorophenyl)-3-(4-methoxyphenyl)-4,5-dihydro-1*H*-pyrazol-1-yl)methanone (D15)

White crystal, mp: 208–209 °C. ^{1}H NMR ($CDCl_3$, 300 MHz) δ: 3.17–3.24 (d, J = 17.4 Hz, 1H), 3.69–3.80 (m, 1H), 3.87 (s, 3H), 4.42–4.47 (d, J = 11.1 Hz, 1H), 4.52–4.56 (m, 1H), 5.64–5.67 (m, 1H), 5.77–5.83 (m, 1H), 6.86–6.91 (m, 3H), 6.95–6.98 (d, J = 9.0 Hz, 2H), 7.02–7.12 (m, 3H), 7.20–7.25 (m, 2H), 7.68–7.71 (d, J = 8.7 Hz, 2H). MS (ESI): 433.15 ($C_{25}H_{22}FN_2O_4$, $[M+H]^+$). Anal. Calcd for $C_{25}H_{21}FN_2O_4$: C, 69.44; H, 4.89; F, 4.39; N, 6.48; O, 14.80. Found: C, 69.26; H, 4.87; N, 6.49.

4.6. Anti-proliferation assay

WM266.4 melanoma cells were cultured in DMEM/10% fetal bovine serum, in 5% CO_2 water saturated atmosphere at 37 °C. Cell suspensions (10,000/mL) were prepared and 100 μL/well dispensed into 96-well plates (Costar) giving 1000 cells/well. The plates were returned to the incubator for 24 h to allow the cells to reattach. These compounds were initially prepared at 20 mM in DMSO. Aliquots (200 μL) were diluted into 20 mL culture medium giving 200 μM, and 10 serial dilutions of 3× prepared. Aliquots (100 μL) of each dilution were added to the wells, giving doses ranging from 100 μM to 0.005 μM. After a further incubated at 37 °C for 24 h in a humidified atmosphere with 5% CO_2, the cell viability was assessed by the conventional 3-(4,5-dimethylthiazol-2-yl)-2,5-diphenyltetrazolium bromide (MTT) reduction assay and carried out strictly according to the manufacturer instructions (Sigma). The absorbance at 590 nm was recorded using LX300 Epson Diagnostic micro-plate reader. Then GI_{50} was calculated using SPSS 13.0 software.

4.7. Kinase inhibitory assay

This V600E mutant B-Raf kinase assay was performed in triplicate for each tested compound in this study. Briefly, 7.5 ng Mouse Full-Length GST-tagged $BRAF^{V600E}$ (Invitrogen, PV3849) was preincubated at room temperature for 1 h with 1 μL drug and 4 μL assay dilution buffer. The kinase assay was initiated when 5 μL of a solution containing 200 ng recombinant human full length, N-terminal His-tagged MEK1 (Invitrogen), 200 μM ATP, and 30 mM $MgCl_2$ in assay dilution buffer was added. The kinase reaction was allowed to continue at room temperature for 25 min and was then quenched with 5 μL 5× protein denaturing buffer (LDS) solution. Protein was further denatured by heating for 5 min at 70 °C. About 10 μL of each reaction was loaded into a 15-well, 4–12% precast NuPage gel (Invitrogen) and run at 200 V, and upon completion, the front, which contained excess hot ATP, was cut from the gel and discarded. The gel was then dried and developed onto a phosphor screen. A reaction that contained no active enzyme was used as a negative control, and a reaction without inhibitor was used as the positive control.

Detection of the effect of compounds on cell based pERK1/2 activity in WM266.4 cells was performed using ELISA kits (Invitrogen) and strictly according to the manufacturer instructions.

4.8. Acute oral toxicity

Five thousand milligrams of compounds **C14** and **D10** per kilogram of bodyweight were administered to ten healthy rats by oral gavage, respectively. The animals were observed for mortality, signs of gross toxicity and behavioral changes at least once daily for 14 days. Bodyweights were recorded prior to administration and again on Day 7 and 14. All animals survived and appeared active and healthy throughout the study. With the exception of one male that exhibited a loss (2%) in body weight between Day 7 and 14, all animals gained bodyweight over the 14-day observation period. There were no signs of gross toxicity or abnormal behavior.

4.9. Docking study

The three-dimensional structures of the aforementioned compounds were constructed using Chem. 3D ultra 12.0 software [Chemical Structure Drawing Standard; Cambridge Soft corporation, USA (2010)], then they were energetically minimized by using MMFF94 with 5000 iterations and minimum RMS gradient of 0.10. The crystal structures of B-Raf kinase domain bound to SB-590885 (PDB code: 2FB8) and bound to SM7 (PDB code: 3PSD) complex were retrieved from the RCSB Protein Data Bank (http://www.rcsb.org/pdb/home/home.do). All bound waters and ligands were eliminated from the protein and the polar hydrogen was added to the proteins. Molecular docking of all thirty compounds as well as **C0** was then carried out using the Discovery Stutio (version 3.1) as implemented through the graphical user interface CDocker protocol.

CDocker is an implementation of a CHARMm based molecular docking tool using a rigid receptor,[25] including the following steps:

(1) A series of ligands conformations are generated using high temperature molecular dynamics with different random seeds.
(2) Random orientations of the conformations are generated by translating the center of the ligand to a specified position within the receptor active site, and making a series of random rotations. A softened energy is calculated and the orientation is kept when it is less than a specified limit. This process repeats until either the desired number of low-energy orientations is obtained, or the test times of bad orientations reached the maximum number.
(3) Each orientation is subjected to simulated annealing molecular dynamics. The temperature is heated up to a high temperature then cooled to the target temperature. A final energy minimization of the ligand in the rigid receptor using non-softened potential is performed.
(4) For each of the final pose, the CHARMm energy (interaction energy plus ligand strain) and the interaction energy alone are figured out. The poses are sorted according to CHARMm energy and the top scoring (most negative, thus favorable to binding) poses are retained. The whole B-Raf kinase domain defined as a receptor and the site sphere was selected based on the original ligand binding location, then the original ligand was removed and the ligands prepared by us were placed during the molecular docking procedure. CHARMm was selected as the force field. The molecular docking was performed with a simulated annealing method. The heating steps were 2000 with 700 of heating target temperature. The cooling steps were 5000 with 300 cooling target temperature. Ten molecular docking poses saved for each ligand were ranked according to their dock score function. The pose with the highest -CDocker energy was chosen as the most suitable pose.

4.10. QSAR model

Among all the 30 compounds, 80% (i.e., 24) were utilized as a training set for QSAR modeling. The remaining 20% (i.e., 6) were

chosen as an external test subset for validating the reliability of the QSAR model by the Diverse Molecules protocol in Discovery Studio 3.1. The selected test compounds were: C3, C8, C15, D4, D5 and D14.

The inhibitory activity of the compounds in literatures [IC_{50} (mol/L)] was initially changed into the minus logarithmic scale [p IC_{50} (mol/L)] and then used for subsequent QSAR analysis as the response variable.

In Discovery Studio, the CHARMm force field is applied and the electrostatic potential together with the *Van der Waals* potential are treated as separate terms. As the electrostatic potential probe, A + le point change is used while distance-dependent dielectric constant is used to mimic the solvent effect. As for the *Van der Waals* potential, a carbon atom with a radius of 1.73 Å is used as a probe.

A partial least-squares (PLS) model is built using energy grids as descriptors. QSAR models were built by using the create 3D QSAR Model protocol in Discovery Studio 3.1.

Acknowledgment

This work was financed by National Natural Science Foundation of China (No. J1103512).

References and notes

1. El-Aza, A. S.; Al-Omar, M. A.; Abdel-Aziz, A. M.; Abdel-Aziz, N. I.; El-Sayed, A. A.; Aleisa, A. M.; Sayed-Ahmed, M. M.; Abdel-Hamide, S. G. *Eur. J. Med. Chem.* **2010**, *45*, 4188.
2. Hoshino, R.; Chantani, Y.; Yamori, T.; Tsuruo, T.; Oka, H.; Yoshida, O.; Shimada, Y.; Ari-I, S.; Wada, H.; Fujimoto, J.; Kohno, M. *Oncogene* **1999**, *18*, 813.
3. Li, N.; Batt, D.; Warmuth, M. *Curr. Opin. Investig. Drugs* **2007**, *8*, 452.
4. Davies, H.; Bignell, G. R.; Cox, C.; Stephens, P.; Edkins, S.; Clegg, S.; Teague, J.; Woffendin, H.; Garnett, M. J.; Bottomley, W.; Davis, N.; Dicks, E.; Ewing, R.; Floyd, Y.; Gray, K.; Hall, S.; Hawes, R.; Hughes, J.; Kosmidou, V.; Menzles, A.; Mould, C.; Parker, A.; Stevens, C.; Watt, S.; Hooper, S.; Wilson, R.; Jayatilake, H.; Gusterson, B. A.; Cooper, C.; Shipley, J.; Hargrave, D.; Pritchard-Jones, K.; Maitland, N.; Chenevix-Trench, G.; Riggins, G. J.; Bigner, D. D.; Palmieri, G.; Cossu, A.; Flanagan, A.; Nicholson, A.; Ho, J. W. C.; Leung, S. Y.; Yuen, S. T.; Weber, B. L.; Seigler, H. F.; Darrow, T. L.; Paterson, H.; Marais, R.; Marshall, C. J.; Wooster, R.; Stratton, M. R.; Futreal, P. A. *Nature* **2002**, *417*, 949.
5. Cohen, Y.; Xing, M.; Mambo, E.; Guo, Z.; Wu, G.; Trink, B.; Beller, U.; Westra, W. H.; Landenson, P. W.; Sidransky, D. *J. Natl. Cancer Inst.* **2003**, *95*, 625.
6. Xu, X.; Quiros, R. M.; Gattuso, P.; Ain, K. B.; Prinz, R. A. *Cancer Res.* **2003**, *63*, 4561.
7. Kalinsky, K.; Haluska, F. G. *Expert Rev. Anticancer Ther.* **2007**, *7*, 715.
8. Dhillon, D. S.; Hagan, S.; Rath, O.; Kolch, W. *Oncogene* **2007**, *26*, 3279.
9. Wan, P. T.; Garnet, M. J.; Roe, S. M.; Lee, S.; Niculescu-Duvaz, D.; Good, V. M.; Jones, C. M.; Marshall, C. J.; Springer, C. J.; Barford, D.; Marais, R. *Cell* **2004**, *116*, 855.
10. Wilhelm, S. M.; Carter, C.; Tang, L. Y.; Wilkie, D.; McNabola, A.; Rong, H.; Chen, C.; Zhang, X. M.; Vincent, P.; McHugh, M.; Cao, Y. C.; Shujath, J.; Gawlak, S.; Eveleigh, D.; Rowley, B.; Liu, L.; Adnane, L.; Lynch, M.; Auclair, D.; Taylor, I.; Gedrich, R.; Voznesensky, A.; Riedl, B.; Post, L. E.; Bollag, G.; Trail, P. A. *Cancer Res.* **2004**, *64*, 7099.
11. Ibrahim, P. N.; Zhang, J.; Cho, H.; Mamo, S.; Bremer, R.; Gillette, S.; Kumar, A.; Fong, D.; Wang, W.; Zhu, Y.-L.; Marimuthu, A.; Suzuki, Y.; Lam, B.; Rice, J.; Tsai, J.; Settachatgul, C.; Shelloe, R.; Cantwell, J.; West, B.; Powell, B.; Habets, G.; Zhang, C.; Artis, D. R.; Hirth, P.; Bollag, G. *Abstr. Pap. Am. Chem. Soc.* **2006**, *232*.
12. McDermott, U.; Sharma, S. V.; Dowell, L.; Greninger, P.; Montagut, C.; Lamb, J.; Archibald, H.; Raudales, R.; Tam, A.; Lee, D.; Rothenberg, S. M.; Supko, J. G.; Sordella, R.; Ulkus, L. E.; Iafrate, A. J.; Maheswaran, S.; Njauw, C. N.; Tsao, H.; Drew, L.; Hanke, J. H.; Ma, X.-J.; Erlander, M. G.; Gray, N. S.; Haber, D. A.; Settleman, J. *Proc. Natl. Acad. Sci. U.S.A.* **2007**, *104*, 19936.
13. King, A. J.; Patrick, D. R.; Batorsky, R. S.; Ho, M. L.; Do, H. T.; Zhang, S. Y.; Kumar, R.; Rusnak, D. W.; Takle, A. K.; Wilson, D. M.; Hugger, E.; Wang, L.; Karreth, F.; Lougheed, J. C.; Lee, J.; Chau, D.; Stout, T. J.; May, E. W.; Rominger, C. M.; Schaber, M. D.; Luo, L.; Lakdawala, A. S.; Adams, J. L.; Contractor, R. G.; Smalley, K. S. M.; Herlyn, M.; Morrissey, M. M.; Tuveson, D. A.; Huang, P. S. *Cancer Res.* **2006**, *66*, 11100.
14. Ridley, R. G.; Hofheinz, W.; Matile, H.; Jaquet, C.; Dorn, A.; Masciadri, R.; Jolidon, S.; Richter, W. F.; Guenzi, A.; Girometta, M. A.; Urwyler, H.; Huber, W.; Thaithong, S.; Peters, W. *Antimicrob. Agents Chemother.* **1846**, *1996*, 40.
15. De, D. Y. D.; Krogstad, F. M.; Byers, L. D.; Krogstad, D. J. *J. Med. Chem.* **1998**, *41*, 4918.
16. Azarifar, D.; Ghasemnejad, H. *Molecules* **2003**, *8*, 642.
17. Blackburn, C.; Duffy, M. O.; Gould, A. E.; Kulkarni, B.; Liu, J. X.; Menon, S.; Nagayoshi, M.; Vos, T. J.; Williams, J. *Bioorg. Med. Chem. Lett.* **2010**, *20*, 4795.
18. Li, C. Y.; Li, Y.; Li, Q. S.; Sun, X. G.; Wei, R.; Gong, H. B.; Zhu, H. L. *Bioorg. Med. Chem.* **2012**, *20*, 3746.
19. Vazquez, M. T.; Rosell, G.; Pujol, M. D. *Farmaco* **1996**, *51*, 215.
20. Harrak, Y.; Rosell, G.; Daidone, G.; Plescia, S.; Schillaci, D.; Pujol, M. D. *Bioorg. Med. Chem.* **2007**, *15*, 4876.
21. Vasquez, M. T.; Rosell, G.; Pujol, M. D. *Eur. J. Med. Chem.* **1997**, *32*, 529.
22. Xu, M. Z.; Lee, W. S.; Han, J. M.; Oh, H. W.; Park, D. S.; Tian, G. R.; Jeong, T. S.; Park, H. Y. *Bioorg. Med. Chem.* **2006**, *14*, 7826.
23. Kirkpatrick, P. *Nat. Rev. Drug Disc.* **2004**, *3*, 299.
24. Newhouse, B. J.; Hansen, J. D.; Grina, J.; Welch, M.; Topalov, G.; Littman, N.; Callejo, M.; Martinson, M.; Galbraith, S.; Laird, E. R.; Brandbuber, B. J.; Vigers, G.; Morales, T.; Woessner, R.; Randolph, N.; Lyssikatos, J.; Olivero, A. *Bioorg. Med. Chem. Lett.* **2011**, *21*, 3488.
25. Wu, G. S.; Robertson, D. H.; Brooks, C. L.; Vieth, M. *J. Comput. Chem.* **2003**, *24*, 1549.